Nanoscale Research Letters
a SpringerOpen Journal

NANO EXPRESS Open Access

# Microplasma illumination enhancement of vertically aligned conducting ultrananocrystalline diamond nanorods

Kamatchi Jothiramalingam Sankaran[1], Srinivasu Kunuku[2], Shiu-Cheng Lou[3], Joji Kurian[4], Huang-Chin Chen[4], Chi-Young Lee[1], Nyan-Hwa Tai[1*], Keh-Chyang Leou[2], Chulung Chen[3] and I-Nan Lin[4*]

**Abstract**

Vertically aligned conducting ultrananocrystalline diamond (UNCD) nanorods are fabricated using the reactive ion etching method incorporated with nanodiamond particles as mask. High electrical conductivity of 275 $\Omega \cdot cm^{-1}$ is obtained for UNCD nanorods. The microplasma cavities using UNCD nanorods as cathode show enhanced plasma illumination characteristics of low threshold field of 0.21 V/μm with plasma current density of 7.06 $mA/cm^2$ at an applied field of 0.35 V/μm. Such superior electrical properties of UNCD nanorods with high aspect ratio potentially make a significant impact on the diamond-based microplasma display technology.

**Keywords:** Ultrananocrystalline diamond nanorods, Reactive ion etching, Microplasma, Electron field emission properties

## Background

Microplasma science and technology is an intersection of plasma science, photonics, and materials science, which offers not only a realm of plasma phenomenology but also device functionality [1-4]. Such plasma-based devices exhibit great potential for a broad spectrum of applications in microdisplays, on-chip frequency standards, materials synthesis, elemental analysis, and detectors of environmentally hazardous or toxic gases or vapors [5-11] But due to the insufficient luminous efficiency of the plasma devices [12], development of a cathode material with efficient emission of secondary electrons for improving the initiation efficiency of plasma illumination is thus called for. Among carbon-based materials, diamond is a promising material for applications in various electronic and microelectromechanical devices due to its unparalleled intrinsic properties such as wide energy band gap, chemical inertness, extreme hardness, high thermal conductivity, and negative electron affinity [13-16]. Moreover, diamond materials have large secondary electron emission efficiency which is especially adept for serving as cathode materials in microplasma devices [17]. Recent reports of *n*-type conductivity [18] and high electron field emission (EFE) characteristics in $N_2$-incorporated ultrananocrystalline diamond (UNCD) films exhibited the potential of such films for cold cathode emitters [19,20]. These materials are expected to be beneficial for maintaining the plasma excitation when serving as cathode materials for the plasma devices.

It is not the intrinsic properties alone but the surface geometry also which serves in defining the properties for potential applications of materials. In spite of retaining the same chemical composition, nanostructured materials exhibit pronounced variations in the properties in comparison with their bulk and film forms. For instance, it has been demonstrated that diamond coatings on silicon nanostructures significantly reduce the turn-on field ($E_0$) of EFE [21,22]. Processing of materials to a desired geometry will depend entirely on the intrinsic properties such as hardness, chemical and/or mechanical stability, etc., of the materials. Nanostructures of extremely hard and chemically inert materials such as diamond and other wide-bandgap materials (GaN, Si) have been obtained by the top-down methods including reactive ion etching (RIE) process with or without mask focus

* Correspondence: nhtai@mx.nthu.edu.tw; inanlin@mail.tku.edu.tw
[1]Department of Materials Science and Engineering, National Tsing-Hua University, Hsinchu, Taiwan 300, Republic of China
Full list of author information is available at the end of the article

Springer

© 2012 Sankaran et al.; licensee Springer. This is an Open Access article distributed under the terms of the Creative Commons Attribution License (http://creativecommons.org/licenses/by/2.0), which permits unrestricted use, distribution, and reproduction in any medium, provided the original work is properly cited.

ion beam milling and bottom-up approaches [23-33]. Owing to practical applications, it is still of great interest to formulate a low-cost, flexible, and relevant method to fabricate diamond nanostructures with high areal density and high uniformity in a desired geometry.

In this letter, we report the fabrication of vertically aligned UNCD nanorods from *n*-type UNCD films by RIE using nanodiamond (ND) particles as a hard etching mask. We observed that the plasma illumination characteristics of a microplasma cavity were markedly enhanced when the UNCD nanorods were used as the cathode materials, as compared with those using the as-grown UNCD films as cathode. The detailed mechanism of the improvement of the plasma illumination characteristics of the nanorods is investigated.

## Methods

UNCD films were grown on Si substrates in a microwave plasma-enhanced chemical vapor deposition system (2.45 GHz 6″ IPLAS-CYRANNUS, Troisdorf, Germany). Prior to deposition, the substrates were ultrasonicated in methanol solution containing the mixture of ND powders (approximately 5 nm) and titanium powders (approximately 325 nm) for 45 min to facilitate the nucleation. The UNCD films were deposited on substrates using $N_2$ (94%)/$CH_4$ (6%) plasma with a microwave power of 1,200 W for 1 h. The pressure and the flow rate were maintained at 50 Torr and 100 sccm, respectively. An external heater was used to heat the substrate to a temperature of about 700°C, where the substrate temperature is measured using a thermocouple (*K* type) embedded in the substrate holder. The obtained UNCD films were designated as $N_2$-UNCD films. The $N_2$-UNCD films were then immersed in a pseudo-stable suspension (ND particles (8 to 10 nm in diameter) and deionized water) and sonicated for 10 min to seed ND particles on the $N_2$-UNCD films surface. The ND particle layer on the $N_2$-UNCD films is dense, which depends on the suspension quality and time of sonication. After masking, the $N_2$-UNCD films were then etched using the RIE process in an $O_2$ (80%)/$CF_4$ (20%) gas mixture at rf power of 150 W for 30 min. In the process, ND particles acted as etching mask for fabricating vertically aligned $N_2$-UNCD nanorods.

The morphologies and microstructures of the samples were examined using field emission scanning electron microscopy (FESEM; JEOL-6500, JEOL Ltd., Tokyo, Japan) and transmission electron microscopy (TEM; JEOL 2100; operated under 200 eV), respectively. The visible Raman ($\lambda = 632.8$ nm; Lab Raman HR800; Jobin Yvon, Inc., NJ, USA) spectroscopic measurements were performed at room temperature. Hall measurements were carried out in a van der Pauw configuration (ECOPIA HMS 3000, Bridge Technology, USA) to confirm *n*-type conductivity of the films. EFE characteristics of the samples were measured using a molybdenum rod with a diameter of 2 mm as anode, and *I-V* characteristics were acquired using Keithley 237 electrometer (Keithley Instruments, Inc., OH, USA). The EFE behavior of the materials was explained using Fowler-Nordheim (F-N) theory [34]. The plasma illumination characteristics of a microcavity, in which an indium tin oxide (ITO)-coated glass was used as anode and the $N_2$-UNCD nanorods were used as cathode, were also investigated. The cathode-to-anode separation was fixed by a Teflon spacer (1.0 mm in thickness). A circular hole about 8.0 mm in diameter was cut out from the Teflon spacer to form a microcavity. The plasma was triggered using a pulsed direct current voltage in bipolar pulse mode in Ar environment at a pressure of 100 Torr.

## Results and discussion

FESEM image of the $N_2$-UNCD films shows highly dense and uniformly distributed needle-like granular structures in the films (not shown). The root-mean square roughness of the surface is about 7 to 10 nm, and the thickness of the films is about 1 μm. The Hall measurements conducted in the van der Pauw configuration showing the electrical conductivity of the $N_2$-UNCD films are found to be $186\,\Omega{\cdot}\mathrm{cm}^{-1}$. Vertically aligned $N_2$-UNCD nanorods are fabricated by subjecting the $N_2$-UNCD films to the RIE process.

Figure 1a shows the FESEM image of the vertically aligned $N_2$-UNCD nanorods with diameters of about 15 to 20 nm and lengths of about 460 nm. Examination of the films using TEM is necessary to explicitly identify the microstructural nature of the materials. The high resolution TEM image of a single nanorod (Figure 1b) taken from the marked squared region in the low magnification TEM micrograph (upper-right inset of Figure 1b) reveals two crystalline carbon phases, diamond (marked squared region 1 in Figure 1b) and graphite (marked squared region 2 in Figure 1b). The image shows a nanorod with a diameter of about 15 nm, surrounded by graphitic phase. The thickness of the graphitic layer can vary from a few atomic layers to approximately 3 nm. The associated selective area electron diffraction (SAED) pattern of the low-magnification TEM micrograph of the $N_2$-UNCD nanorods (upper-right inset of Figure 1b) also clearly shows the presence of two different crystalline phases: a diamond phase (sharp rings designated as $d_{111}$, $d_{220}$, and $d_{311}$) and a graphitic phase (central diffused ring). In addition, the Fourier transformed (FT) diffractogram corresponding to the region 1 of the structure image ($FT_1$) clearly illustrates the diamond phase, whereas the FT image corresponding to the region 2 ($FT_2$) indicates that these curved parallel fringes correspond to a few layers of

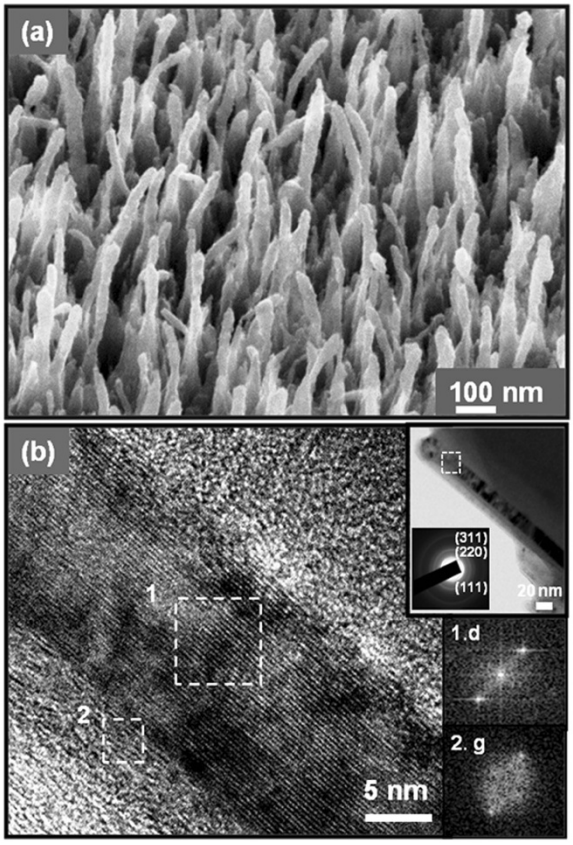


**Figure 1 FESEM morphology and TEM images of $N_2$-UNCD nanorods.** (**a**) FESEM morphology of the $N_2$-UNCD nanorods, which are fabricated from $N_2$-UNCD films grown using $N_2$ (94%)/$CH_4$ (6%) plasma at 700°C, using RIE etching process with nanodiamond particles as masking materials. (**b**) High resolution TEM image of $N_2$-UNCD nanorod with the upper-right inset showing the low magnification TEM image of $N_2$-UNCD nanorod and the corresponding SAED pattern. The insets 1 and 2 show the Fourier-transformed diffractogram (FT images) of the areas marked as 1 and 2, indicating that the UNCD nanorods are encased in a thin shell of graphite content of around 2 to 3 nm thickness. d, diamond; g, graphite.

graphitic phase. These results confirm that the nanorods are encapsulated by a sheath of graphitic phase. The microstructural studies of $N_2$-UNCD films confirmed that this graphitic content is formed during the growth of the films [35]. The presence of abundant CN species in the $N_2/CH_4$ plasma, which was observable in the optical emission spectra (not shown), may preferentially induce the formation of nanorod, along with the graphitic phase encasing the nanorods [36].

The nanorods are subjected to Hall measurements with the measuring probes directly in contact with the nanorods (inset a of Figure 2), and the electrical conductivity increases to about $275\,\Omega\cdot\mathrm{cm}^{-1}$ (Figure 2). The visible Raman spectrum of the $N_2$-UNCD nanorods is shown in the inset b of Figure 2. The spectrum is deconvoluted using the multi-peak Lorentzian fitting method. Two prominent resonance peaks are observed in the spectrum. The broadened Raman peak at approximately 1,335 $cm^{-1}$ is attributed to the *D* band, which arises due to disordered carbon, while the peak observed at approximately 1,597 $cm^{-1}$, assigned as the *G* band, is due to the graphitic phase in the nanorods [37], which is in accord with the TEM observation. It must be noted that the absence of a sharp feature at approximately 1,332 $cm^{-1}$ is due to the use of visible Raman spectroscopy, which is more sensitive towards $sp^2$-bonded carbon. The $N_2$-UNCD nanorods exhibit high electrical conductivity due to the increase in the content of $sp^2$ carbon bonding in the nanorods.

The EFE measurements were carried out on the $N_2$-UNCD nanorods, and the results are shown in Figure 3 with the inset a showing the F-N plot. An applied field at a current density of 10 $\mu A/cm^2$ was taken as the $E_0$. The $N_2$-UNCD nanorods require only $(E_0)_{\mathrm{nanorod}} = 2.04$ V/μm to turn on the EFE process and reach an EFE current density $(J_e)_{\mathrm{nanorod}}$ of 4.84 $mA/cm^2$ at an applied field of 3.2 V/μm. Such EFE properties are markedly superior to those of the $N_2$-UNCD films with $(E_0)_{\mathrm{film}}$ of 4.70 V/μm and $(J_e)_{\mathrm{film}}$ of 3.47 $mA/cm^2$ at 8.8 V/μm applied field (not shown). The relationships among the current density ($J_e$), electric field ($E$), work function ($\phi$), and field enhancement factor ($\beta$) of an emitter are expressed by the F-N equation: $J_e = (Ab^2E^2/\phi)\ \exp\left(-B\phi^{3/2}/bE\right)$, where $A = 1.54 \times 10^{-6}$A eV $V^{-2}$ and $B = 6.83 \times 10^9 \mathrm{eV}^{-3/2}\mathrm{V\ m}^{-1}$. We fit the high field segments of the F-N curve to the above equation and the results of the fitting are shown as straight segment in the inset a of Figure 3, illustrating that the EFE data fit the F-N model very well. We assume that the $\phi$ value of diamond is assumed as 5.0 eV [38] for estimating the $\beta$ value of $N_2$-UNCD nanorods, which is $\beta_{\mathrm{nanorod}} = 1{,}945$ from the F-N slope. The value of $\beta_{\mathrm{nanorod}}$ obtained is larger than that of the $N_2$-UNCD films ($\beta_{\mathrm{film}} = 624$), the enhanced value being due to the electrical field at the nanorod tips.

Figure 4 shows the series of photographs of the plasma devices at different applied electric fields. These photographs show that the microplasma devices using the $N_2$-UNCD nanorods as cathode can be triggered by a voltage of 210 V, and the intensity of the plasma increases monotonously with the applied voltage. The plasma current density of $N_2$-UNCD nanorods $((J_e)_{\mathrm{nanorod}})$ also exhibits a similar increase with the increase of applied electric field and reaches 7.06 $mA/cm^2$ at an applied field of 0.35 V/μm. The $(J_e)_{\mathrm{nanorod}}$ is larger than that of the plasma current density $((J_e)_{\mathrm{film}} = 5.30$ $mA/cm^2$ at an applied field of 0.34 V/μm) of $N_2$-UNCD films (not shown). The threshold field $(E_{\mathrm{th}})_{\mathrm{nanorod}}$ for triggering the plasma corresponds to an applied field of $(E_{\mathrm{th}})$

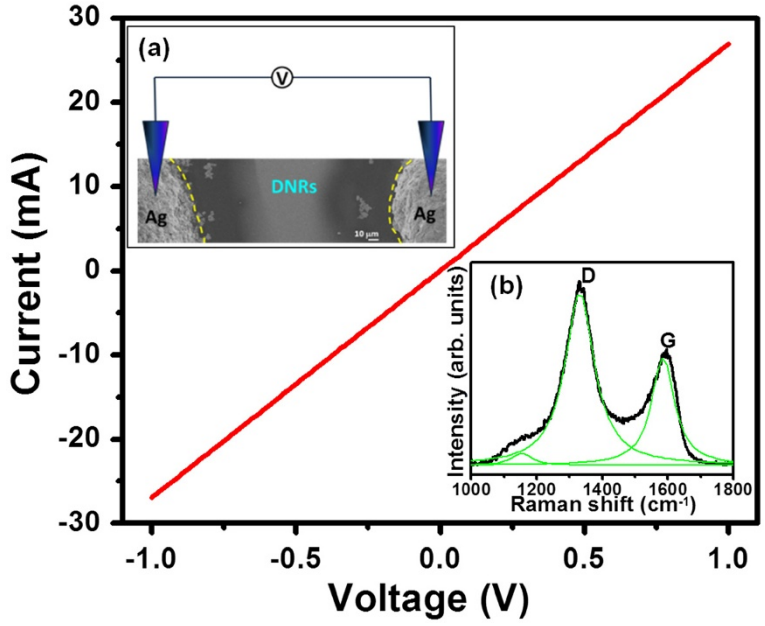


**Figure 2 Current–voltage characteristics and visible-Raman spectrum of $N_2$-UNCD nanorods.** The current–voltage characteristics, which are obtained using Hall measurements with the measuring probes directly in contact with the top of the nanorods (inset **a**), reveal that the $N_2$-UNCD nanorods possess good electrical conductivity of 275 $\Omega \cdot cm^{-1}$. Inset (**b**) shows the visible Raman spectrum of the $N_2$-UNCD nanorods. d, diamond; g, graphite.

$_{nanorod}$ = 0.21 V/μm, which is smaller than the $E_{th}$ value of $N_2$-UNCD film-cathoded microplasma devices (not shown). To evaluate the stability of the plasma illumination from $N_2$-UNCD nanorods, the current was monitored over a period of 7,000 s with a constant applied voltage of 250 V (inset b of Figure 3). The plasma $(J_e)_{nanorod}$ of 4.74 mA/cm$^2$ is upheld for a period of 6,445 s and shows high life-time stability in comparison

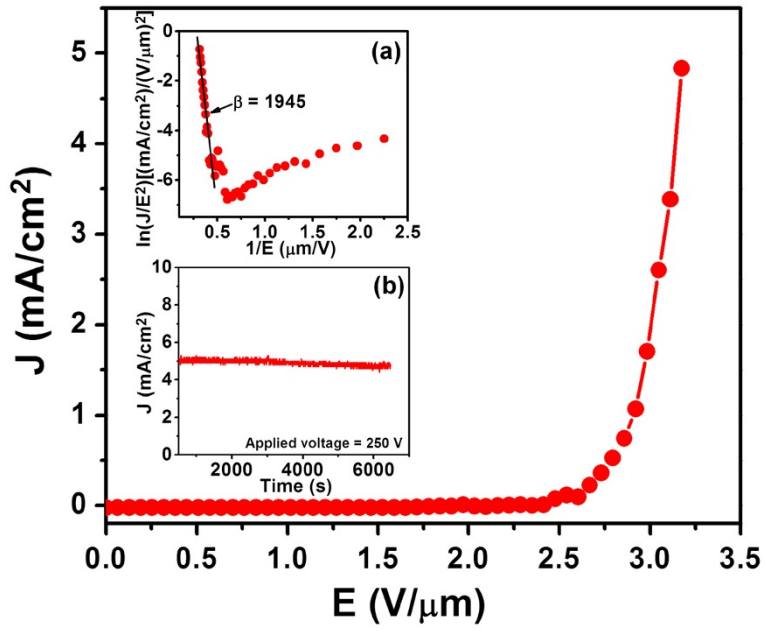


**Figure 3 The electron field emission properties of the $N_2$-UNCD nanorods.** Inset (**a**) shows the corresponding Fowler-Nordheim plot. Inset (**b**) shows the plasma illuminating current stability measurement of a microplasma cavity, which utilized the $N_2$-UNCD nanorods as cathode and ITO glass as anode.

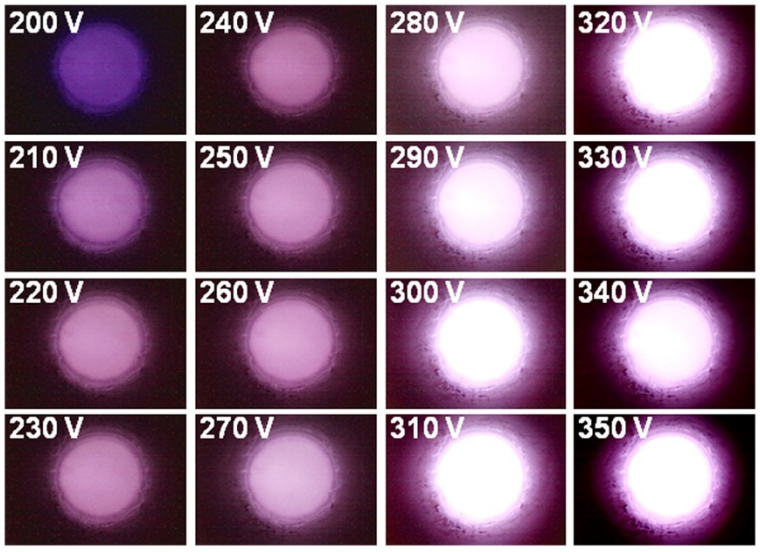


**Figure 4 Plasma illumination characteristics of $N_2$-UNCD nanorods.** The photographs of plasma illumination characteristics of a microplasma cavity which utilized the $N_2$-UNCD nanorods as cathode and ITO glass as anode.

with that of the $N_2$-UNCD films as well as bare Si. Apparently, the better plasma performance of the microplasma cavity using $N_2$-UNCD nanorods as cathode, as compared with that using $N_2$-UNCD film as cathode (not mentioning that of the cavity with the bare Si used as cathode) can be ascribed to the superior EFE properties besides the high secondary electron emission efficiency for the $N_2$-UNCD nanorod materials.

It should be noted that the electric field required to trigger the Ar plasma is much smaller than the $E_0$ for inducing the EFE process for both the $N_2$-UNCD nanorods and $N_2$-UNCD films. The primary reason for such a phenomenon is that the Ar plasma can be triggered whenever the electrons emitted from the cathodes reach a kinetic energy larger than the ionization energy of the Ar species (14.7 eV). Superior EFE properties provide the low ignition threshold for the microplasma easily. After the initiation of the Ar plasma, the cathode materials mainly serve as the source of secondary electrons for maintaining the ignition of the plasma. Better EFE properties of the $N_2$-UNCD nanorods no longer show significant superiority in maintaining the plasma in the microcavity.

## Conclusions

In summary, ND particles dispersed on smooth and highly conducting $N_2$-UNCD films can be utilized as an etching mask for the fabrication of vertically aligned $N_2$-UNCD nanorods. These $N_2$-UNCD nanorods show superb plasma illumination characteristics of low threshold field = 0.21 V/μm with high current density of 7.06 mA/cm$^2$ at an applied field of 0.35 V/μm. The excellent performance of the $N_2$-UNCD nanorods as cathode for the microplasma devices is mainly attributed to the unique granular structure of nanorods and a high proportion of graphitic phase surrounding each nanorod. The utilization of $N_2$-UNCD nanorods enhances the illumination performance of the microplasma devices that can be applied to a broad spectrum of applications in microplasma display technologies.

#### Competing interests

The authors declare that they have no competing interests.

#### Authors' contributions

KJS and NHT carried out the growth, electrical conductivity, and electron field emission studies of $N_2$-UNCD films. SK, JK, and KCL carried out the fabrication of $N_2$-UNCD nanorods using RIE process and Raman spectroscopy studies. SCL and CC carried out the microplasma illumination studies. HCC, CYL, and INL carried out the TEM investigation on $N_2$-UNCD nanorods. All authors read and approved the final manuscript.

#### Authors' information

KJS is a Ph.D. student of the Department of Materials Science and Engineering, National Tsing-Hua University, Hsinchu, Taiwan. SK is a Ph.D. student of Department of Engineering and System Science of the same university. SCL is a Ph.D. student of the Department of Photonics Engineering, Yuan Ze University, Chung-Li, Taiwan. JK is a post doctoral fellow in the Department of Physics, Tamkang University, Tamsui, Taiwan. HCC is a post doctoral fellow in the Department of Materials Science and Engineering, National Tsing-Hua University, Hsinchu, Taiwan. CYL and NHT are professors in the Department of Materials Science and Engineering of the same university. KCL is a professor in the Department of Engineering and System Science of the same university. CC is a professor in the Department of Photonics Engineering, Yuan Ze University, Chung-Li, Taiwan. INL is a professor in the Department of Physics, Tamkang University, Tamsui, Taiwan.

#### Acknowledgement

The authors would like to thank the National Science Council, Republic of China, for the support of this research through the project numbers NSC99-2119-M-032-003-MY2 and NSC98-2221-E-007-045-MY3.

**Author details**
[1]Department of Materials Science and Engineering, National Tsing-Hua University, Hsinchu, Taiwan 300, Republic of China. [2]Department of Engineering and System Science, National Tsing-Hua University, Hsinchu, Taiwan300, Republic of China. [3]Department of Photonics Engineering, Yuan Ze University, Chung-Li, Taiwan 32003, Republic of China. [4]Department of Physics, Tamkang University, Tamsui, Taiwan 251, Republic of China.

Received: 18 July 2012 Accepted: 2 September 2012
Published: 25 September 2012

**References**

1. Eden JG, Park SJ, Ostrom NP, McCain ST, Wagner CJ, Vojak BA, Chen J, Liu C, von Allmen P, Zenhausern F, Sadler DJ, Jensen C, Wilcox DL, Ewing JJ: **Microplasma devices fabricated in silicon, ceramic, and metal/polymer structures: arrays, emitters and photodetectors.** *J Phys D: Appl Phys* 2003, **36:**2869–2877.
2. Park SJ, Chen J, Wagner CJ, Ostrom NP, Liu C, Eden JG: **Microdischarge arrays: a new family of photonic devices.** *IEEE J Sel Top: Quantum Electron* 2002, **8:**387–394.
3. Eden JG, Park SJ, Ostrom NP, Chen KF: **Recent advances in microcavity plasma devices and arrays: a versatile photonic platform.** *J Phys D: Appl Phys* 2005, **38:**1644–1648.
4. Becker KH, Schoenbach KH, Eden JG: **Microplasmas and applications.** *J Phys D: Appl Phys* 2006, **39:**R55–R70.
5. Meng LG, Liu CL, Liang HF, Liang ZH: **Microplasma array devices with coplanar electrodes operating in neon.** *Phys. Lett. A* 2008, **372:**6504–6508.
6. Awad SH, Qian HC: **Deposition of duplex $Al_2O_3$/TiN coatings on aluminum alloys for tribological applications using a combined microplasma oxidation (MPO) and arc ion plating (AIP).** *Wear* 2006, **260:**215–222.
7. Yang ZS, Shirai H, Kobayashi T, Hasegawa Y: **Synthesis of Si nanocones using rf microplasma at atmospheric pressure.** *Thin Solid Films* 2007, **515:**4153–4258.
8. Kanazawa S, Daidai R, Akamine S, Ohkubo T: **Generation of microplasma jet at atmospheric pressure using a modified waveguide-based plasma torch.** *Surf Coat Technol* 2008, **202:**5275–5279.
9. Guchardi R, Hauser PC: **Capacitively coupled microplasma for on-column detection of chromatographically separated inorganic gases by optical emission spectrometry.** *J Chromatogr A* 2004, **1033:**333–338.
10. Hozumi Y, Seto T, Hirasawa M, Tsuji M, Okuyama A: **Kinetics of microplasma atmospheric ion generation correlated with discharge current.** *J. Electrostatics* 2008, **67:**1–6.
11. Michels A, Tombrink S, Vautz W, Miclea M, Franzke J: **Spectroscopic characterization of a microplasma used as ionization source for ion mobility spectrometry.** *Spectrochim Acta B* 2007, **62:**1208–1215.
12. Chen KF, Ostrom NP, Park SJ, Eden JG: **One quarter million (500 × 500) pixel arrays of silicon microcavity plasma devices: luminous efficacy above6 lumens/watt with Ne/50% Xe mixtures and a green phosphor.** *Appl Phys Lett* 2006, **88:**061121–061123.
13. Isberg J, Hammersberg J, Johnsson E, Wikstrom T, Twitchen DJ, Whitehead AJ, Coe SE, Scarsbrook GA: **High carrier mobility in single-crystal plasma-deposited diamond.** *Science* 2002, **297:**1670–1672.
14. Masuda H, Yasui K, Watanabe M, Nishio K, Rao TN, Fujishima A: **Fabrication of ordered diamond/metal nanocomposite structure.** *Chem Lett* 2000, **10:**1112–1113.
15. Kim YD, Choi W, Wakimoto H, Usami S, Tomokage H, Ando T: **Direct observation of electron emission site on boron-doped polycrystalline diamond thin films using an ultra-high-vacuum scanning tunneling microscope.** *Appl Phys Lett* 1999, **75:**3219–3221.
16. Zhou D, McCauley TG, Qin LC, Krauss AR, Gruen DM: **Synthesis of nanocrystalline diamond thin films from Ar–CH4 microwave plasma.** *J Appl Phys* 1998, **83:**540–543.
17. Stacey A, Prawer S, Rubanov S, Ahkvlediani R, Michaelson S, Hoffman A: **The effect of temperature on the secondary electron emission yield from single crystal and polycrystalline diamond surfaces.** *Appl Phys Lett* 2009, **95:**262109(1–3).
18. Bhattacharyya S, Auciello O, Birrell J, Carlisle JA, Curtiss LA, Goyette AN, Gruen DM, Krauss AR, Schlueter J, Sumant A, Zapol P: **Synthesis and characterization of highly-conducting nitrogen-doped ultrananocrystalline diamond films.** *Appl Phys Lett* 2001, **79:**1441–1443.
19. Joseph PT, Tai NH, Lee CY, Niu H, Pong WF, Lin IN: **Field emission enhancement in nitrogen-ion-implanted ultrananocrystalline diamond films.** *J Appl Phys* 2008, **103:**043720(1–7).
20. Chen YC, Tai NH, Lin IN: **Substrate temperature effects on the electron field emission properties of nitrogen doped ultra-nanocrystalline diamond.** *Diam Relat Mater* 2008, **17:**457–461.
21. Tzeng YF, Liu KH, Lee YC, Lin SJ, Lin IN, Lee CY, Chiu HT: **Fabrication of an ultra-nanocrystalline diamond-coated silicon wire array with enhanced field-emission performance.** *Nanotechnology* 2007, **18:**435703(1–5).
22. Tzeng YF, Lee CY, Chiu HT, Tai NH, Lin IN: **Electron field emission properties on ultra-nano-crystalline diamond coated silicon nanowires.** *Diam Relat Mater* 2008, **17:**1817–1820.
23. Zhang WJ, Wu Y, Wong WK, Meng XM, Chan CY, Bello I, Lifshitz Y, Lee ST: **Structuring nanodiamond cone arrays for improved field emission.** *Appl Phys Lett* 2003, **83:**3365–3367.
24. Zhang WJ, Meng XM, Chan CY, Wu Y, Bello I, Lee ST: **Oriented single-crystal diamond cones and their arrays.** *Appl Phys Lett* 2003, **82:**2622–2624.
25. Zhang WJ, Wu Y, Chan CY, Wong WK, Meng XM, Bello I, Lifshitz Y, Lee ST: **Structuring single- and nano-crystalline diamond cones.** *Diam Relat Mater* 2004, **13:**1037–1043.
26. Wang Q, Wang ZL, Li JJ, Huang Y, Li YL, Gu CZ, Cui Z: **Field electron emission from individual diamond cone formed by plasma etching.** *Appl Phys Lett* 2006, **89:**063105(1–3).
27. Hsu CH, Lo HC, Chen CF, Wu CT, Hwang JS, Das D, Tsai J, Chen LC, Chen KH: **Generally applicable self-masked dry etching technique for nanotip array fabrication.** *Nano Lett* 2004, **4:**471–475.
28. Yoshida H, Urushido T, Miyake H, Hiramatsu K: **Formation of GaN self-organized nanotips by reactive ion etching.** *Jpn. J. Appl. Phys* 2001, **40**(Part 2):L1301–L1304.
29. Shenderova OA, Padgett CW, Hu Z, Brenner DW: **Diamond nanorods.** *J Vac Sci Technol B* 2005, **23:**2457–2464.
30. Barnard AS: **Structural properties of diamond nanowires: theoretical predictions and experimental progress.** *Rev Adv Mater Sci* 2004, **6:**94–119.
31. Shang N, Papakonstantinou P, Wang P, Zakharov A, Palnitkar U, Lin IN, Chu M, Stamboulis A: **Self-assembled growth, microstructure, and field-emission high performance of ultrathin diamond nanorods.** *ACS Nano* 2009, **2:**1032–1038.
32. Sun L, Gong J, Zu D, Zhu Z, He S: **Diamond nanorods from carbon nanotubes.** *Adv Mater* 2004, **16:**1849–1853.
33. Vlasov II, Lebedev OI, Ralchenko VG, Goovaerts E, Bertoni G, Tendeloo GV, Konov VI: **Hybrid diamond-graphite nanowires produced by microwave plasma chemical vapor deposition.** *Adv Mater* 2007, **19:**4058–4062.
34. Fowler RH, Nordheim L: **Electron emission in intense electric fields.** *Proc R Soc London, Ser A* 1928, **119:**173–181.
35. Sankaran KJ, Kurian J, Chen HC, Dong CL, Lee CY, Tai NH, Lin IN: **Origin of needle-like granular structure for ultrananocrystalline diamond films grown in $N_2/CH_4$ plasma.** *J Phys D: Appl Phys* 2012, **45:**365303–365311.
36. Teii K, Ikeda T: **Conductive and resistive nanocrystalline diamond films studied by Raman spectroscopy.** *Diam Relat Mater* 2007, **16:**753–756.
37. Xiao X, Birrell J, Gerbi JE, Auciello O, Carlisle JA: **Low temperature growth of ultrananocrystalline diamond.** *Appl Phys Lett* 2004, **96:**2232–2239.
38. Liu J, Zhirnov VV, Myers AF, Wojak GJ, Choi WB, Hren JJ, Wolter SD, McClure MT, Stoner BR, Glass JT: **Field emission characteristics of diamond coated silicon field emitters.** *J Vac Sci Technol B* 1995, **13**(2):422–426.

doi:10.1186/1556-276X-7-522
**Cite this article as:** Sankaran *et al.*: **Microplasma illumination enhancement of vertically aligned conducting ultrananocrystalline diamond nanorods.** *Nanoscale Research Letters* 2012 **7**:522.